Supporting Information for Coupled Yu-Shiba-Rusinov states in molecular dimers on $NbSe_2$

Shawulienu Kezilebieke,[†] Marc Dvorak,[‡] Teemu Ojanen,[*,†] and Peter Liljeroth[*,†]

†*Department of Applied Physics, Aalto University School of Science, P.O.Box 15100, 00076 Aalto, Finland*

‡*Centre of Excellence in Computational Nanoscience (COMP) and Department of Applied Physics, Aalto University, P.O.Box 11100, 00076 Aalto, Finland*

E-mail: Email:teemuo@boojum.hut.fi; Email:peter.liljeroth@aalto.fi

Methods

Sample preparation. Sample preparation and subsequent STM experiments were carried out in an ultrahigh vacuum system with a base pressure of $\sim 10^{-10}$ mbar. The $2H$–$NbSe_2$ single crystal (HQ Graphene, the Netherlands) was cleaved in situ by attaching a tape to the crystal surface and pulling the tape in vacuum in the load-lock chamber using the sample manipulator. CoPC molecules (Sigma-Aldrich) was deposited from an effusion cell held at 390°C onto a freshly cleaved $NbSe_2$ at room temperature.

STM measurements. After the CoPc deposition, the sample was inserted into the low-temperature STM (Unisoku USM-1300) and all subsequent experiments were performed at $T = 4.2$ K. STM images were taken in the constant current mode. $\mathrm{d}I/\mathrm{d}V$ spectra were recorded by standard lock-in detection while sweeping the sample bias in an open feedback

loop configuration, with a peak-to-peak bias modulation of $50 - 100$ μV at a frequency of 709 Hz. The procedure for acquiring a spectrum was as follows: the tip was moved over the molecule at the imaging parameters (e.g. $V = 0.6$ V and $I = 5$ pA), the tip-sample distance was reduced by changing the setpoint to e.g. 200 pA at 100 mV. Finally, after disconnecting the feedback at the beginning the $\mathrm{d}I/\mathrm{d}V$ spectrum, the tip-sample distance was decreased by a further $50 - 100$ pm (z_{offset}) to increase the signal to noise ratio. The detailed numbers are given in the figure captions.

The $NbSe_2$ tip was prepared by indenting the tip into the $NbSe_2$ surface by a few nanometers while applying a voltage of 10V. Manipulation of the CoPc was carried out by placing the tip above the centre of the molecule with a bias voltage of 0.1 V and the current was increased to 1 nA with the feedback engaged. The tip was then dragged towards the desired location.

DFT calculations. Density functional theory calculations were performed with the FHI-AIMS computational package[1,2] and the PBE generalized gradient approximation for the exchange-correlation functional.[3] We used the standard "light" numerical settings and basis sets of numeric atomic-centered orbitals tested and recommended by FHI-AIMS. Periodic $NbSe_2$ supercells were sampled with a 2×2 k-point grid centred on the Γ point. Van der Waals interactions were included by the post-SCF Tkatchenko-Scheffler correction.[4] Before computing the electronic structure, all atomic forces were relaxed to < 0.01 eV/Å.

Adsorption geometry of CoPc

The adsorption site of CoPc can be determined from atomically resolved STM images (Fig. S2). The STM feedback current was increased at the top and bottom parts of the image to allow resolving the $NbSe_2$ lattice. While scanning over the molecules, the setpoint current was reduced in order not to accidentally manipulate the molecules. Extrapolating the atomically resolved $NbSe_2$ lattice (Se is visible) allows estimating the CoPc adsorption site. Both

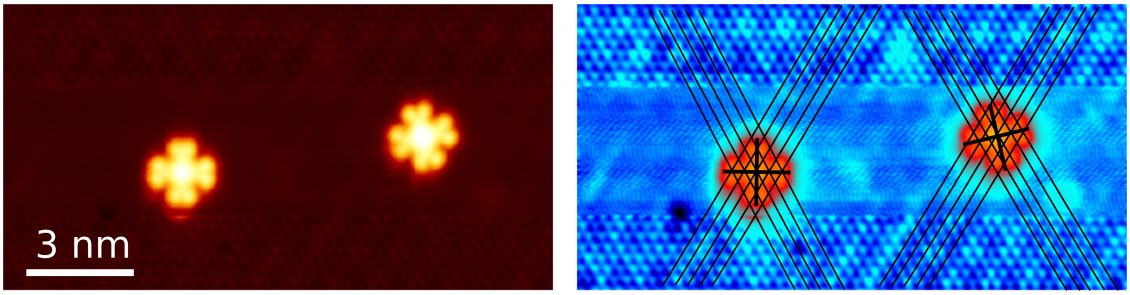

Figure S1: STM image of two CoPc molecules ($V = 50$ mV, $I = 1$ nA on $NbSe_2$ and $V = 0.7$ V, $I = 3$ pA on CoPc). The STM feedback current was reduced of the CoPc to avoid their accidental manipulation.

molecules are adsorbed with the cobalt centre directly on top of a selenium atom in agreement with the DFT calculations.

Spectra over a single CoPc molecule

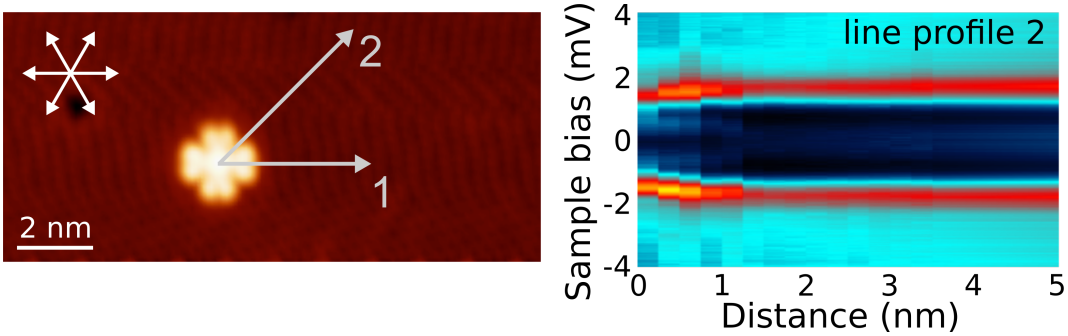

Figure S2: Spectra along a line over a CoPc molecule (profile 2). Spectra along line 1 are shown in Fig. 1. Feedback setpoint: $V = 100$ mV, $I = 200$ pA, $z_{\text{offset}} = 0$. The colour scale is between $0 - 0.03$ μS.

We have carried out experiments to probe the nature of the individual YSR states. In addition to the spectra along line profile 1 shown in the main manuscript, we have additional data along profile 2 at a 45° angle w.r.t. profile 1 (Fig. S2). This data suggests that the YSR state has shorter decay along this direction. It can also been seen that the YSR resonances shift towards the gap edge, which is difficult to consolidate with the picture of the YSR states being eigenstates of the impurity-surface complex. This effect is also seen (to a lesser extent) on the profile 1 in Fig. 1e of the main text. To check if this effect could be caused by the

interaction with the STM tip, we have measured spectra at different tip-sample distances in the middle of a CoPc molecule (Fig. S3). We start all the experiments at a distance determined by the set-point conditions and approach the tip by a distance of z_{offset} before recording the spectrum.

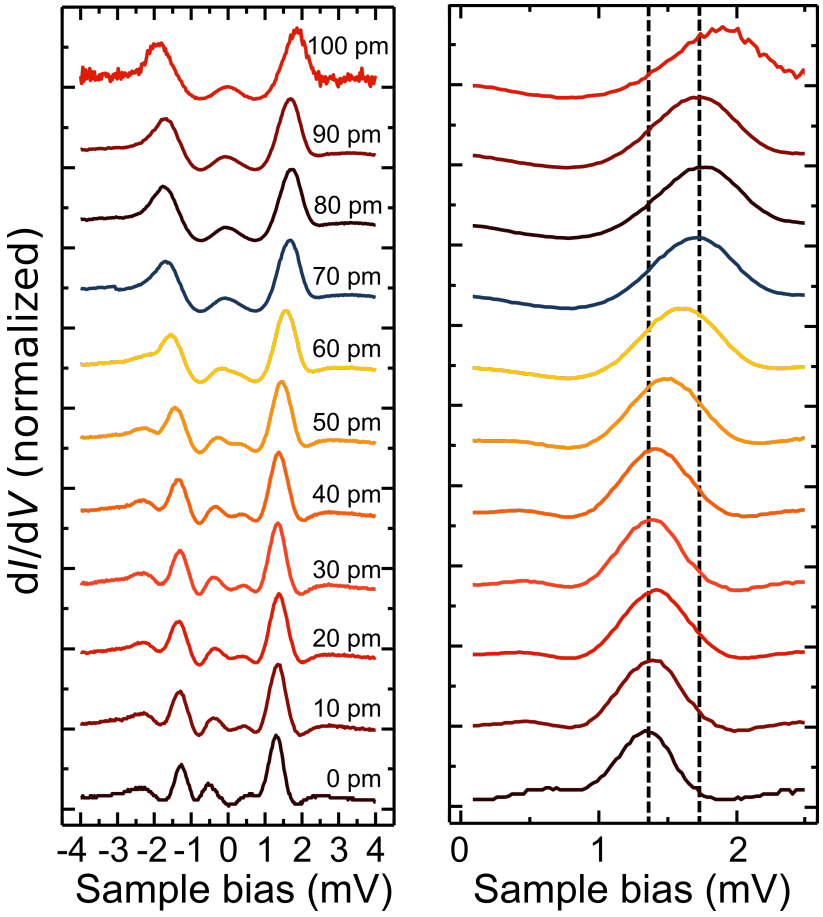

Figure S3: dI/dV spectra (normalized) recorded over the middle of a CoPc molecule at different tip-molecule distances. $z_{\text{offset}} = 0$ pm corresponds to the set-point conditions at $V = 20$ mV, $I = 300$ pA.

dI/dV spectra acquired at different tip-sample distances show a shift of the YSR resonance to higher bias starting at roughly $z_{\text{offset}} = 30 - 40$ pm. At around $z_{\text{offset}} = 80$ pm, the YSR resonance has merged with the superconducting coherence peak at the gap edge. The spectrum recorded at $z_{\text{offset}} = 100$ pm has significantly higher noise and broader resonances compared to the other spectra, and the molecule becomes unstable under the tip at larger values of z_{offset}. On the bare substrate, varying the tip-sample distance has no effect on the

shape or position of the superconducting coherence peaks.

This measurement clearly indicates that there are considerable interactions between the tip and the CoPc molecules at reduced tip-sample distances. This interaction modifies the coupling with the underlying $NbSe_2$ substrate, as evidenced by the continuous shift of the YSR resonances as a function of the tip-sample distance. Specifically, as the YSR resonance shifts towards the SC gap edge, the tip-molecule interaction reduces the coupling of the magnetic moment with the superconducting substrate. Speculating, we are likely to be in the attractive force regime of the tip-sample interactions and as the molecule is weakly (van der Waals) bonded on the surface, the tip-sample interaction could have an effect on its adsorption height. Alternatively, the screening from the metallic tip could have an effect on the scalar potential at the impurity site, which would also have an effect on the YSR energy.

These experiments allow us to conclude that under our normal conditions (spectra in the manuscript are recorded in conditions similar to $z_{\mathrm{offset}} = 0$), the tip-sample interactions do not play a significant role when we carry out the $\mathrm{d}I/\mathrm{d}V$ spectroscopy in the middle of the molecule. However, as the tip moves towards the sample close to the edges of the molecule, some shifts of the YSR resonances may occur due to the tip-sample interaction.

In order to shed further light into the YSR states on single CoPc molecules, we have mapped them out by performing grid spectroscopy (recording a complete $\mathrm{d}I/\mathrm{d}V$ spectrum at each scan point). These experiments are quite demanding due to the mobility of the molecules and we carried them out in STM feedback to have enough signal on the substrate and not to have too much current on the molecule. In addition, we used as low currents as possible to minimize tip-molecule interactions and to reduce the changes of accidental lateral manipulation of the molecule. The results are shown in Fig. S4, which displays raw data $\mathrm{d}I/\mathrm{d}V$ slices at the energies corresponding to the YSR (panel c) and the superconducting coherence peaks (panel d) and the same results normalized to take into account the varying tip height (panels e and f).

The YSR peaks are mostly localized in the centre of the molecule (Fig. S4e), with faint

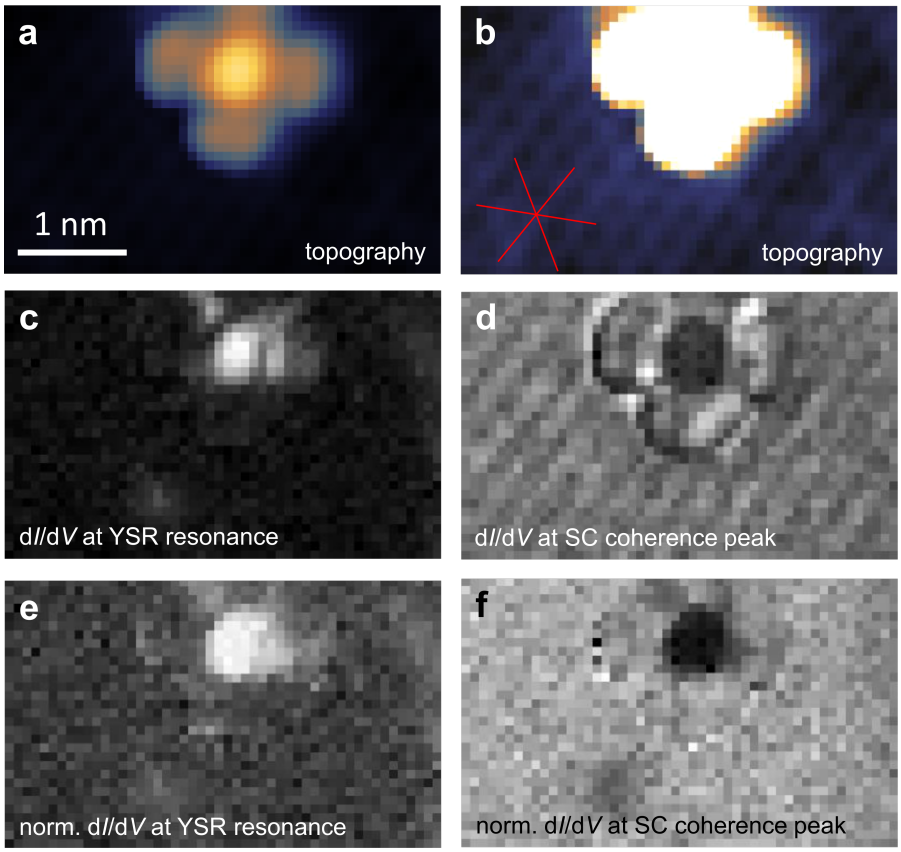

Figure S4: Grid spectroscopy on an individual CoPc molecule. (a) Topography image acquired simultaneously with the $\mathrm{d}I/\mathrm{d}V$ spectra. (b), Topography at enhanced contrast to show the atomically resolved underlying $NbSe_2$ lattice. (c) $\mathrm{d}I/\mathrm{d}V$ slice at the bias corresponding to the YSR peak (positive bias). Gray scale is between $0-0.03$ μS. (d) $\mathrm{d}I/\mathrm{d}V$ slice at the bias corresponding to the superconducting coherence peak (positive bias). Gray scale is between $0-0.02$ μS. (e, f) Maps corresponding to panels c and d, where the $\mathrm{d}I/\mathrm{d}V$ signal has been normalized by the current at the beginning of the spectrum. Set-point $V = 500$ mV, $I = 5$ pA, $z_{\mathrm{offset}} = 100$ pm.

tails in different directions that seem to coincide with the principal lattice directions of the underlying $NbSe_2$ substrate and not with the molecular symmetry. There is a corresponding dip in the SC coherence peak intensity (Fig. S4f). While the normalization removes most of the effect of the molecular backbone (which will has an effect on the tunneling barrier between the tip and sample), this is still faintly visible in (Fig. S4e and f, which complicates quantitative analysis of the $\mathrm{d}I/\mathrm{d}V$ maps.

STM manipulation

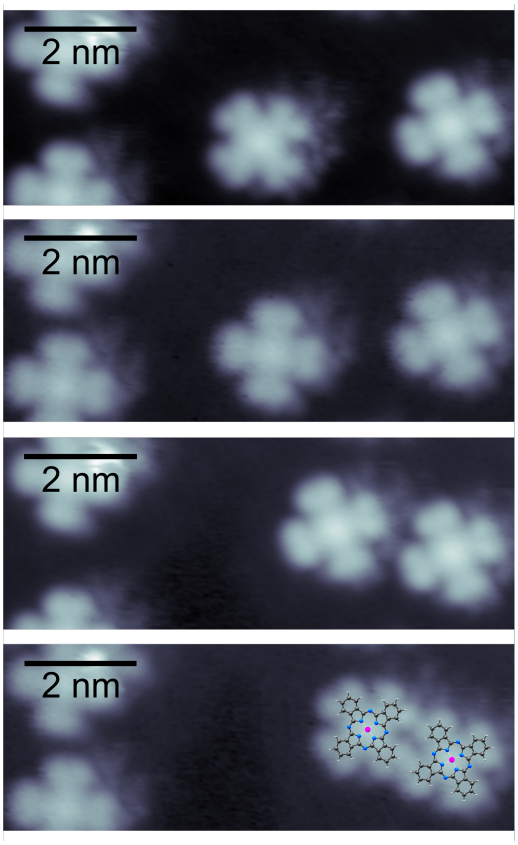

Figure S5: Lateral molecular manipulation of CoPc on $NbSe_2$. Subsequent STM images of CoPc molecules after one of the molecules was laterally manipulated by the STM tip.

CoPc molecules are weakly adsorbed on the $NbSe_2$ surface, making it easy to laterally manipulate them by the STM tip (Fig. S5. We successfully constructed molecular dimers with different separations by STM manipulation. Manipulation of the CoPc was carried out by placing the tip above the centre of the molecule at 0.1 V bias voltage and increasing the current to 1 nA with the feedback engaged. The tip was then dragged towards the desired location. In order to avoid the potential variability caused by the adsorption orientation, we always manipulated one molecule of the dimer and recorded the spectrum on the one which had not been moved. In this way, we have made sure that the target molecule is always in the same adsorption configuration. Figure S5 shows a series of manipulation steps demonstrating that we only move the target molecule on the surface. The structural models

of the CoPc molecules overlaid on the last panel show that the molecules are still not in "contact".

Deconvolution of the dI/dV spectra

The tunneling current I at bias V can be calculated from[5]

$$I(V) = \int_{-\infty}^{\infty} \rho_{\mathrm{t}}(\epsilon)\rho_{\mathrm{s}}(\epsilon + eV)\Big(f(\epsilon) - f(\epsilon + eV)\Big)d\epsilon \tag{1}$$

where ρ_{t} and ρ_{s} are the tip and substrate densities of states and f is the Fermi function. $NbSe_2$ has an anisotropic gap structure,[6] which we approximated by sum of gapped DOS with some broadening and an additional gaussian component, similar to the expressions used before for modelling STM experiments with SC tips[7,8]

$$\rho_{\mathrm{SC}}(E) = A_1 \mathrm{Re}\left(\frac{|E|}{\Big((|E| + i\gamma_1)^2 - \Delta_1^2\Big)^{1/2}}\right) + A_2 \exp(-(|E| - \Delta_2)^2/(2\gamma_2^2)) \tag{2}$$

where $A_{1,2}$, $\Delta_{1,2}$ and $\gamma_{1,2}$ are fitted from the spectra measured on a clean $NbSe_2$ substrate with a superconducting tip. We can fit the experimental spectra extremely well as shown in Fig. S6 using the same parameters for the bulk $NbSe_2$ substrate and for the superconducting tips prepared by controlled contacts with the clean substrate. After this, using the same tip with a known ρ_{t}, we extract the substrate DOS on the CoPc molecules by a direct numerical deconvolution of Eq. (1). This is an example of a Fredholm integral equation of the first kind and can be solved numerically through a matrix equation.[9]

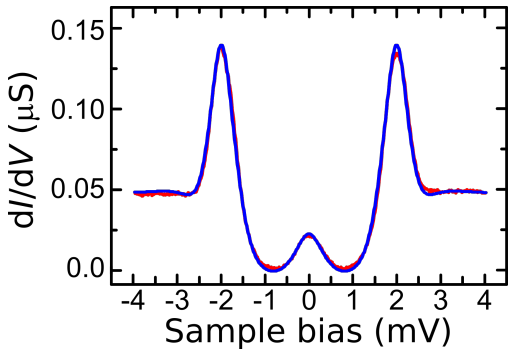

Figure S6: Deconvolution of the superconducting tip DOS. Experimental dI/dV spectrum (red line) compared with the fit to Eq. (1) (blue line) with $\Delta_1 = 0.98$ meV, $\Delta_2 = 1.01$ meV, $\gamma_1 = 0.16$ meV, $\gamma_2 = 0.27$ meV, $A_1 = 0.659$, $A_2 = 0.341$, and $T_{\text{eff}} = 4.27$ K. Feedback set-point $V = 100$ mV, $I = 50$ pA, $z_{\text{offset}} = 100$ pm.

Theoretical description of coupled magnetic moments

Lattice model

In this supplement, we outline in detail the theoretical modelling of coupled Yu-Shiba-Rusinov states on the surface of $NbSe_2$. The starting point of the analysis is a lattice description of an s-wave superconductor with Hamiltonian

$$H_0 = \sum_{ij,\sigma} \frac{t_{ij}}{2}(c^\dagger_{i\sigma}c_{j\sigma} + c^\dagger_{j\sigma}c_{i\sigma}) + \sum_{i,\sigma} \Delta(c_{i\sigma}c_{i\bar{\sigma}} + c^\dagger_{i\bar{\sigma}}c^\dagger_{i\sigma}), \tag{3}$$

where t_{ii} is an on-site potential and t_{ij} $(i \neq j)$ are hopping elements between the lattice sites. The second term describes superconducting pairing of electrons with the pairing gap Δ. The operators $c^\dagger_{i\sigma}, c_{j\sigma}$ create and destroy electrons at lattice site i with spin σ and obey the usual fermionic anticommutation relations. We assume a triangular lattice where the band structure of $NbSe_2$ can be reproduced by an appropriate choice of parameters t_{ij}. The magnetic impurities are assumed to be local and described by the Hamiltonian

$$H_{\text{imp}} = -J_1\mathbf{S}_1 \cdot C^\dagger_{n_1}\sigma C_{n_1} - J_2\mathbf{S}_2 \cdot C^\dagger_{n_2}\sigma C_{n_2} + V_1 C^\dagger_{n_1}C_{n_1} + V_2 C^\dagger_{n_2}C_{n_2}, \tag{4}$$

where $J_i, \mathbf{S}_i$ are a magnetic coupling and a classical spin vector of an impurity at lattice position n_i. Here, we have introduced Pauli matrices $\sigma = (\sigma_x, \sigma_y, \sigma_z)$ and the second-quantized spinor operators $C_{n_i} = (c_{i\uparrow}, c_{i\downarrow})^T$. In addition to the magnetic coupling, the impurities may also perturb the superconductor with additional scalar potential parametrized by V_1 and V_2.

The standard method of solving the eigenstates of the Hamiltonian $H_0 + H_{\mathrm{imp}}$ is to generalize the problem to particle-hole space with the basis $\Psi_i = (c_{i\uparrow}, c_{i\downarrow}, c^\dagger_{i\downarrow}, -c^\dagger_{i\uparrow})^T$ and to diagonalize the Bogoliubov-de Gennes Hamiltonian

$$H_{\mathrm{BdG}} = \frac{t_{ij}}{2}\tau_z \otimes I_{2\times 2} + \Delta\delta_{ij}\tau_x \otimes I_{2\times 2} \quad - \quad J_1\delta_{n_1 n_1} I_{2\times 2} \otimes \mathbf{S}_1 \cdot \sigma - J_2\delta_{n_2 n_2} I_{2\times 2} \otimes \mathbf{S}_2 \cdot \sigma + V_1 \quad \delta_{n_1 n_1}\tau_z \otimes I_{2\times 2} + V_2\delta_{n_2 n_2}\tau_z \otimes I_{2\times 2}, \tag{5}$$

which is a $4N_1 \times 4N_2$ matrix where N_1 and N_2 are the number of lattice sites in the direction of the primitive lattice vectors of a triangular lattice. We have solved the Bogoliubov-de Gennes problem $H_{\mathrm{BdG}}\Psi = E\Psi$ for a tight-binding model of $NbSe_2$ with a finite on-site, nearest-neighbour and next-nearest neighbour hoppings. The energy spectrum is symmetric with respect to zero with a gap 2Δ. Inside the gap we recover two pairs of states, corresponding to the bonding and antibonding combinations of individual YSR states. In the calculations presented in the main text, we have used values of -100 meV for the on-site and -125 meV for the nearest- and next-nearest neighbour hopping parameters[10] and $\Delta = 1$ meV, $J_1 S_1 = J_2 S_2 = 35$ meV, $V_1 = V_2 = 0$ on a lattice with $N_1 = N_2 = 400$.

Continuum model

To gain qualitative insight of the bound states of the coupled magnetic impurities we have also studied a 2D continuum model with a circular Fermi surface. In the continuum description

the Bogoliubov-de Gennes Hamiltonian takes the form

$$H_{\mathrm{BdG}} = \varepsilon_k \tau_z \otimes I_{2\times 2} + \Delta \tau_x \otimes I_{2\times 2} - J\delta(\mathbf{r}-\mathbf{r}_1) I_{2\times 2} \otimes \mathbf{S}_1 \cdot \sigma - J\delta(\mathbf{r}-\mathbf{r}_2) I_{2\times 2} \otimes \mathbf{S}_2 \cdot \sigma, \quad (6)$$

where $\varepsilon_k = \frac{k^2}{2m} - \mu$ is the kinetic energy measured from the Fermi surface while the other terms are straightforward counterparts of those present in the lattice model. In the case of a single impurity, the standard calculation leads to a pair of subgap states with energies $E = \frac{1-\alpha^2}{1+\alpha^2}$, with the dimensionless coupling $\alpha = \pi\nu JS$ which contains the density of states at the Fermi level ν. Since we are not including a spin-orbit coupling, the single impurity results does not depend on the orientation of the impurity moment. While the two-spin problem does not admit a simple closed form analytical expression, the eigenstates can be solved, for example, by the methods of Ref.[11] This leads to four subgap states $\pm E_1$ and $\pm E_2$ where the energy splitting $|E_1 - E_2|$ depends on the relative angle of the two impurity moments. The splitting is maximal for parallel moments and vanishes for antiparallel moments. As illustrated in Fig. S7, the intermediate cases interpolate between the two cases in a nonlinear manner. Thus one expects a four-peak structure for coupled spins, even with random orientation between the magnetic moments. Due to the slow decay $\sim \frac{1}{\sqrt{r}}$ of 2D Shiba wavefunctions for distances smaller than the superconducting coherence length, the splitting decays slowly. Finally, as the experiments and the lattice calculations reveal, the isotropic Fermi surface cannot adequately capture coupling of two moments which varies strongly in a lattice scale.

Angular averaging of the YSR splitting

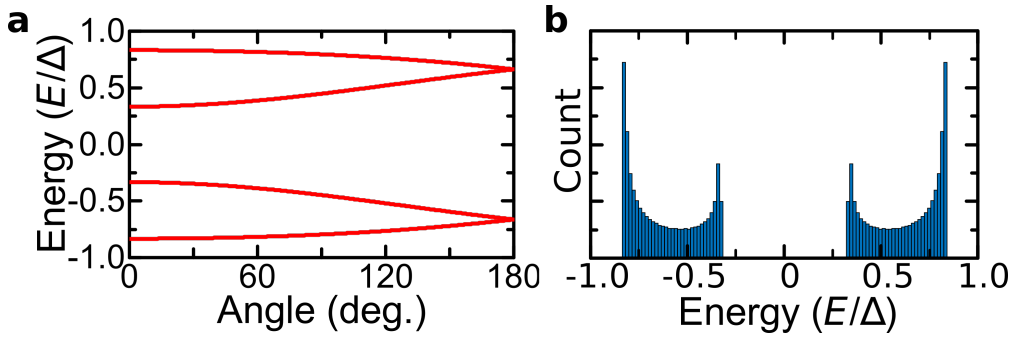

Figure S7: Angular averaging of the YSR splitting. (a) YSR state energies as a function of the angle of the magnetic moments of the two impurities according to the continuum model ($k_{\mathrm{F}}a = 3.8$, $\alpha = 0.5$). (b) Same data presented as a histogram, which shows that majority of the angles result in a YSR splitting very close to the maximum value. This would result in clearly split resonances in the experimental spectra.

YSR splitting as a function of the dimer separation and angle

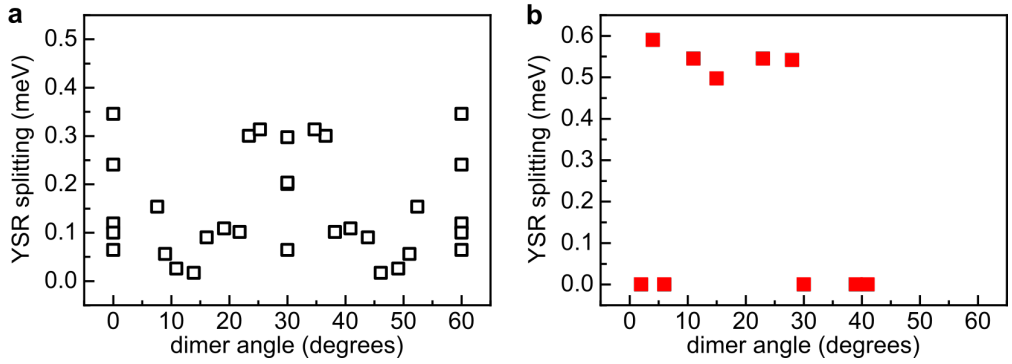

Figure S8: (a) Theoretical plot of the YSR splitting vs. the angle between the dimer axis and one of the principal directions of the substrate. (b) Experimental data (corresponding to the experimental data in Fig. 3c).

References

(1) Blum, V.; Gehrke, R.; Hanke, F.; Havu, P.; Havu, V.; Ren, X.; Reuter, K.; Scheffler, M. Ab initio molecular simulations with numeric atom-centered orbitals. *Comput. Phys. Commun.* **2009**, *180*, 2175 – 2196.

(2) Havu, V.; Blum, V.; Havu, P.; Scheffler, M. Efficient integration for all-electron electronic structure calculation using numeric basis functions. *J. Comput. Phys.* **2009**, *228*, 8367 – 8379.

(3) Perdew, J. P.; Burke, K.; Ernzerhof, M. Generalized Gradient Approximation Made Simple. *Phys. Rev. Lett.* **1996**, *77*, 3865–3868.

(4) Tkatchenko, A.; Scheffler, M. Accurate molecular van der Waals interactions from ground-state electron density and free-atom reference data. *Phys. Rev. Lett.* **2009**, *102*, 073005.

(5) Tersoff, J.; Hamann, D. R. Theory of the scanning tunneling microscope. *Phys. Rev. B* **1985**, *31*, 805–813.

(6) Hudson, E. W. Investigating high-Tc superconductivity on the atomic scale by scanning tunneling microscopy. Ph.D. thesis, University of California at Berkeley, 1999.

(7) Franke, K. J.; Schulze, G.; Pascual, J. I. Competition of superconducting phenomena and Kondo screening at the nanoscale. *Science* **2011**, *332*, 940–944.

(8) Ruby, M.; Heinrich, B. W.; Pascual, J. I.; Franke, K. J. Experimental Demonstration of a Two-Band Superconducting State for Lead Using Scanning Tunneling Spectroscopy. *Phys. Rev. Lett.* **2015**, *114*, 157001.

(9) Twomey, S. On the Numerical Solution of Fredholm Integral Equations of the First Kind by the Inversion of the Linear System Produced by Quadrature. *J. ACM* **1963**, *10*, 97–101.

(10) Flattè, M. E.; Reynolds, D. E. Local spectrum of a superconductor as a probe of interactions between magnetic impurities. *Phys. Rev. B* **2000**, *61*, 14810–14814.

(11) Kim, Y.; Zhang, J.; Rossi, E.; Lutchyn, R. M. Impurity-Induced Bound States in Superconductors with Spin-Orbit Coupling. *Phys. Rev. Lett.* **2015**, *114*, 236804.